Friction reduction in piston ring cylinder liner contact using textured surfaces

PLEASE CITE THE PUBLISHED VERSION

PUBLISHER

LUBMAT 2014

VERSION

AM (Accepted Manuscript)

PUBLISHER STATEMENT

LICENCE

REPOSITORY RECORD

Morris, Nicholas J., Michael Leighton, Ramin Rahmani, Miguel De la Cruz, and Homer Rahnejat. 2019. "Friction Reduction in Piston Ring Cylinder Liner Contact Using Textured Surfaces". figshare. https://hdl.handle.net/2134/18838.

Friction reduction in Piston Ring Cylinder Liner Contact using Textured Surfaces

N. Morris, M. Leighton, R. Rahmani, M. De la Cruz, H. Rahnejat

Wolfson School of Mechanical & Manufacturing Engineering,
Loughborough University, Leicestershire, UK

ABSTRACT

The automotive industry is increasingly required to meet tough emission standards such as Euro 6 which will be implemented in September 2014. Improved fuel efficiency is envisaged to be a direct contributory factor in reducing harmful emissions among other factors. Therefore, reduction of frictional losses in contact conjunctions is progressively an important issue. The compression ring-bore conjunction is responsible for consuming almost 5% of fuel energy. One intensely researched area is enhancement of tribological performance through surface texturing of contacting solid surfaces in order to retain micro-reservoirs of lubricant in regions which are prone to poor lubrication, for example in piston-cylinder system [1,2].

The current work comprises of a validated numerical model which has been created for analysis of surface texturing in the piston ring cylinder liner contact. The model employs a two dimensional solution of Reynolds equation as well as the inclusion of Greenwood and Tripp boundary friction model [3]. The model is used to investigate the underlying mechanism of lubrication with textured surfaces. The understanding of surface texturing developed during this study enables design and positioning of textured patterns in piston ring - cylinder liner contact.

Keywords: Piston ring, Cylinder liner, Laser surface texturing, Surface engineering, Tribology

1. INTRODUCTION

The piston compression ring-bore contact accounts for 5% of input fuel energy [4]. This is significant for such a small conjunction. With ever-increasing costs and stricter emerging legislation much attention is directed towards reducing the parasitic losses.

The piston ring is one of the most challenging tribological contacts on the account of transient nature of the regime of lubrication during a typical engine cycle [5]. At the reversal points adverse tribological conditions are experienced due to piston reversal (thus cessation of lubricant entraining motion into the contact), particularly in transition between the compression to power stroke with high pressures acting behind the top compression ring inducing boundary interactions [6]. Laser texturing can be used to reduce friction in reciprocating contacts[1,2,7-9]. This paper describes how direct measurements of friction are obtained from a reciprocating slider bearing test rig. The results from the reciprocating slider rig are used to validate a numerical model which predicts the effect of surface texture features. The numerical model is then used for the analyses of the top compression ring in a fired engine. Numerical results for surface texturing the piston ring cylinder liner contact are reported.

2. EXPERIMENTAL SET UP

A precision reciprocating slider bench test rig has been developed [10]. A thin sliding strip (representative of compression ring thickness) with a face-width contact profile is loaded against and slides upon a flat plate. The plate is mounted upon precision low friction bearings and is allowed to float, when dragged by the sliding strip. An electric motor is directly coupled to the loaded and sliding strip via low friction and an almost backlash-free leadscrew. Piezo-resistive force sensors measure the inertial force of the floating plate, which is due to generated contact friction as:

$$\sum F = -F_t = ma \tag{1}$$

This arrangement is analogous to floating liner in situ direct measurement of friction from a motored or fired IC engine as reported, for example, by Gore et al [11].

The actual sliding speed of the strip is measured by a rotational laser Doppler vibrometer. The thin strip is made of stainless steel grade 330 C and is hardened to 62HRC. The flat plate is made of EN 14 steel, electroplated by a 20μm thick Ni-SiC coating. The surface is then ground and polished (Table 2).

2.1 Laser surface texturing
A laser surface texturing process was used to etch chevron-shaped textures onto the flat plate similar to those created by Costa and Hutchings [12]. An SPI 50Watt Fibre laser (table 1) was used to create the surface features.

Table 1. Laser data

Parameter	Value (Unit)
Beam Width	0.030 (mm)
Feed speed	0.25 (mm/s)
Pulse Width	0.500 (ms)
Frequency	1687 (Hz)
Power	16 (W)
Shielding Gas	Nitrogen @ 0.5 MPa

The plates were polished for a short period of time after the Laser surface texturing process to remove any splatter or debris left protruding from the surface. The images in Figure 1 show typical laser-etched chevrons obtained through the Alicona Infinite Focus Microscope.
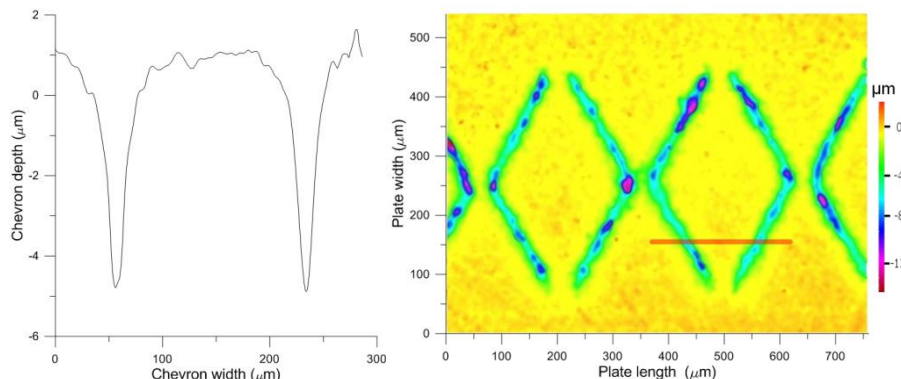

Figure 1: Image of chevrons on test plate

The chevron depth, ring face profile and Surface roughness of the plate and strip were measured. The chevrons have a thickness-to-depth ratio of 0.11 (representative of an optimised ratio as demonstrated in [8]) although some variation in the chevron depth is produced during the laser surface texturing process. The laser surface texturing process produces chevrons with a cross-sectional profile similar to that of a parabola (figure 1), therefore, modelled accordingly. If l is a typical chevron's cross-sectional width, h_d is the depth of the chevron at its centre and x_0 its centre position, then the profile can be described by:

$$\left(\frac{x-x_0}{l/2}\right)^2 + \frac{y}{h_d} = 1 \tag{2}$$

2.2 Test protocol
Before the start of each set of sliding tests, the load cells were calibrated and surface topography of the contact surfaces were measured. Figure 2 shows typical topography of the strip's contacting face-width. A drop of oil was applied onto the flat liner plate using a syringe. The oil was evenly spread across the surface. An initial running-in period was allowed prior to each test. After each test the surfaces of the strip and the floating plate were measured again.
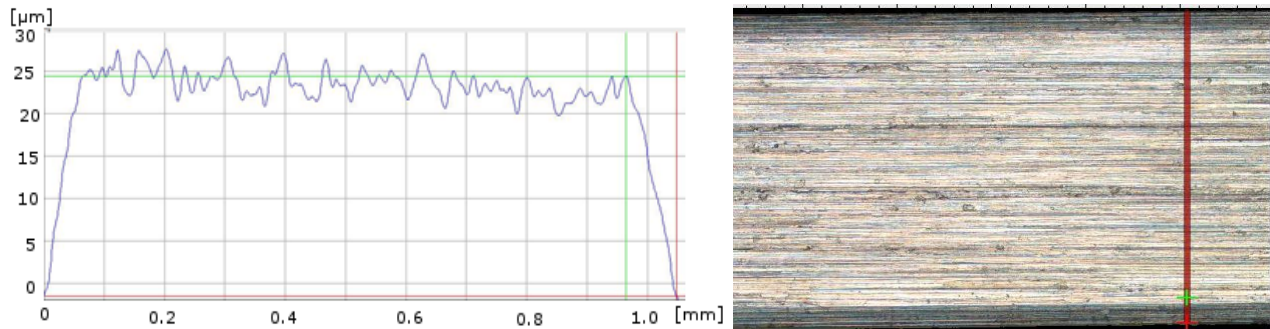
Figure 2: Measured ring face profile

3. NUMERICAL METHODOLOGY

A combined numerical and experimental approach is undertaken to ascertain the effectiveness of laser textured surfaces in retention of a lubricant film and improving hydrodynamic load carrying capacity, as well as reducing friction. Previous experimental evidence has suggested that in the case of piston ring-cylinder liner system 2-4% reduction in friction is attained [1,9]. Furthermore, Balakrishnan et al [13] carried out numerical analysis for piston skirt-textured cylinder bore conjunction and showed improved oil retention through creation of textured chevron-type reservoirs at the top dead centre. The predictions for piston skirt-liner oil film thickness showed remarkable agreement with measurement of the film thickness under the same conditions using ultrasonic sensors [14]. However, measurements of either oil film thickness or friction were not obtained for the much narrower ring-bore conjunction. This paper uses a thin strip slider, representing a segment of circumferentially conforming ring against a flat floating plate of finite width. A quasi-3D analysis can be carried out, using Reynolds equation:

$$\frac{\partial}{\partial x}\left(\frac{\rho h^3}{6\eta}\frac{\partial p}{\partial x}\right) + \frac{d}{dy}\left(\frac{\rho h^3}{6\eta}\frac{\partial p}{\partial y}\right) = (U)\frac{\partial}{\partial x}(\rho h) + 2\frac{\partial}{\partial t}(\rho h)$$

(3)

Reynolds equation is solved together with the film thickness equation, representing the gap shape (Figure 3):

$$h(x, y, t) = h_0(t) + h_s(x, y) + h_t(x, y)$$ (4)

where, h_0 is the minimum film thickness, h_s is the ring face profile and h_t describes the profile of surface features.

The ring face-width profile h_s is measured, and only varies in the x-direction (direction of entraining motion). For the purpose of numerical analysis, the film profile in figure 3 is created using the following set of equations.

$$h_s(x) = \begin{cases} -sx + g & if \ x \le q \\ 0 & if \ q < x < r \\ sx - g & if \ x \ge r \end{cases}$$

(5)

where, s is the gradient with respect to ring face-width, g is the film profile at $x=0$ (the intercept) and r and q refer to the edge and flat land film shape.
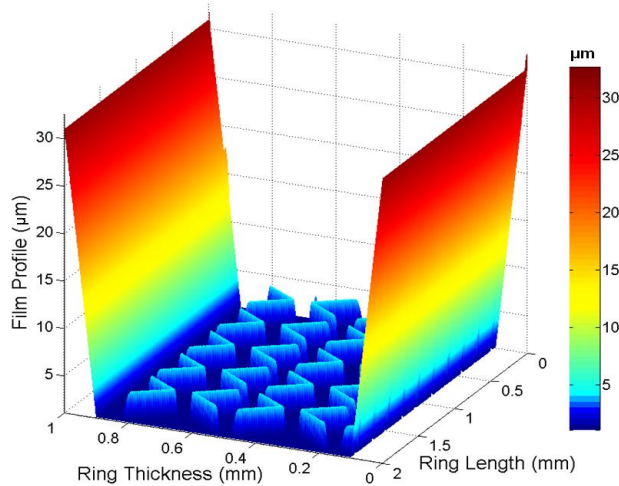
3

Figure 3: Film Shape with chevrons

Due to the relatively low load applied, there is negligible localised deflection of the contacting surfaces, indeed a mixed-hydrodynamic regime of fluid film lubrication is expected. The combination of low load and low lubricant entrainment simulates load-kinematic conditions at TDC reversals under assumed isothermal conditions (such as cold start-up or a motored engine condition). Solution of equations (3) and (4) yields the lubricant film thickness and the hydrodynamic load carrying capacity as:

$$W_h = \int_0^l \int_0^b p \, dx dy \tag{6}$$

A fully flooded inlet is assumed, as the surface of the *floating* plate is provided with a layer of free surface film ahead of the sliding contact. However, low sliding speed is often insufficient to entrain a volume of lubricant into the contact. Thus, a mixed regime of lubrication is anticipated. The outlet boundary conditions are those of Swift-Stieber with assumed atmospheric vaporisation pressure at the film rupture point .The inlet pressure at the front face of the strip is set to atmospheric pressure. Only a segment of the whole strip width in the y-direction (direction of lubricant side-leakage) was included in the model to keep the computational time to an acceptable level. Therefore, symmetric boundary conditions in the transverse direction are used. Thus, the boundary conditions are:

$$p = p_{in} \quad at \quad x = -b/2 \tag{7}$$

$$p = p_c, \quad \frac{dp}{dx} = 0 \quad at \quad x = x_c \tag{8}$$

$$\left.\frac{\partial p}{\partial y}\right|_{(x,0)} = \left.\frac{\partial p}{\partial x}\right|_{(x,l)} = 0 \tag{9}$$

During reciprocating motion some degree of asperity interactions is expected. The mixed and boundary regimes of lubrication are accounted for using the Greenwood and Tripp [3] asperity contact model. The load carried by the asperities is given by equation (10), where E' is the composite Young's modulus of elasticity of the contacting surfaces, and $\zeta k \sigma$ and σ/k are the roughness parameters.

$$W_a = \frac{16\sqrt{2}}{15} \pi (\zeta k \sigma)^2 \sqrt{\frac{\sigma}{k}} E' A F_{5/2}(\lambda) \tag{10}$$

and the statistical function takes the following form

$$F_j(\lambda) = \frac{1}{2\pi} \int_\lambda^\infty (s-\lambda)^j exp\left(-\frac{s^2}{2}\right) ds \tag{11}$$

The sum of the viscous and asperity loads gives the load carrying capacity as:

$$W_T = W_h + W_a \tag{12}$$

The convergence criterion for the numerical analysis is the load balance; between the applied load and that carried by the contact as:

4

$$\frac{|F-W_T|}{F} \leq \varepsilon \tag{13}$$

where, F is the applied load and ε is the error tolerance.

An iterative procedure is followed, if the criterion is not met, by altering the initially guessed value of h_0. The generated viscous friction is given as:

$$F_v = \int_0^l \int_0^b \tau \, dxdy \tag{14}$$

where, assuming no side leakage:

$$\tau = -\frac{h}{2}\frac{\partial p}{\partial x} + \frac{\eta(U_1-U_2)}{h} \tag{15}$$

Boundary friction contribution comprises two parts, as it is assumed that a thin layer of absorbed lubricant resides on the asperity summits and acts in accordance with the non-Newtonian Eyring shear stress τ_0. There is also boundary shear strength of cold-welded asperity pairs on the contiguous counterfaces; ξ, which for a ferrous oxide layer has the value of 0.17 [15].

$$F_b = \tau_0 A_a + \xi W_a \tag{16}$$

The asperity contact area A_a for typical asperity geometry and assumed Gaussian distribution can be obtained from equation (17) considering the general form of statistical function, $F_2(\lambda)$ as [3,15]:

$$A_a = \pi^2(\zeta k\sigma)^2 A F_2(\lambda) \tag{17}$$

The total friction becomes:

$$F_t = F_v + F_b \tag{18}$$

4. RESULTS

The input data for the numerical model is provided in Table 2. The measured sliding speed has a mean value of 24.42 mm/s (±0.06 mm/s).

Table 2. Parameters used in numerical analysis

Parameter	Value
Lubricant viscosity (Pa.s)	0.1583
Ring face width (mm)	1
Ring surface roughness (µm) Ra, Rq	0.511, 0.709
Liner surface roughness (µm) Ra, Rq	0.172, 0.105
Stroke length (mm)	80 (max)
Applied load (N)	0.8
Ring length (mm)	32

The generated pressure distribution is shown in Figure 4. The pressure profile has two distinct features. There is a wedge effect and a trough at the inlet to each chevron facing lubricant entrainment. These act as reservoirs, thus causing low pressure regions. For the chevrons facing opposite to the direction of entrainment there is sharp rise in generated pressures (pressure perturbation). These pressure perturbations are reminiscent of micro-elastohydrodynamic effect. Pressure fluctuations enhance load carrying capacity of the contact relative to the nominally smooth surface.
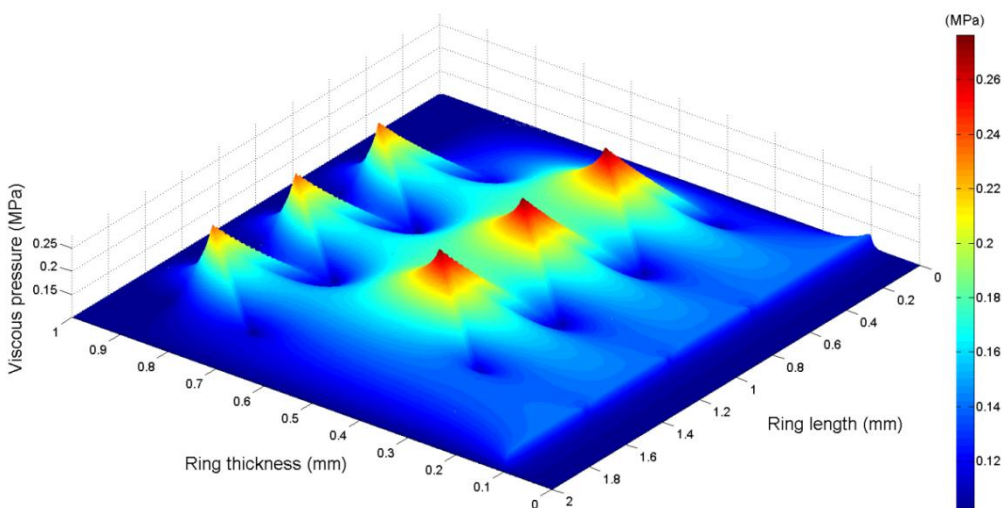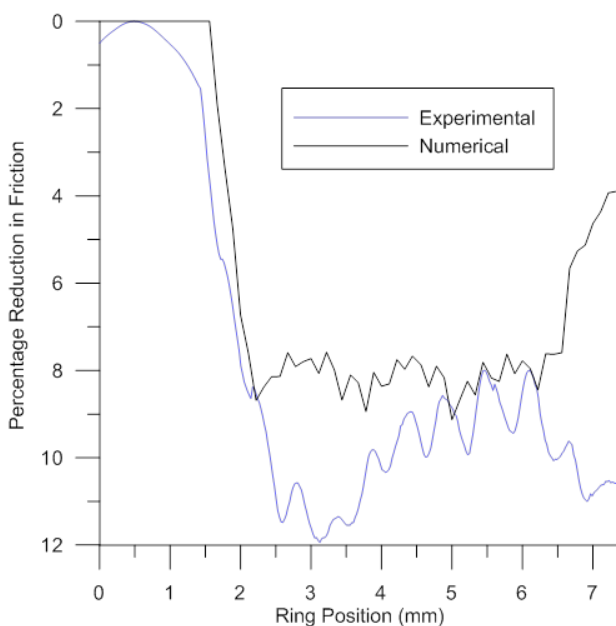
Figure 4: Viscous pressure distribution

Figure 5: Predicted and measured reduced friction with chevron textures

Therefore, as the strip traverses the introduced chevrons an increase in the load carrying capacity is predicted. Hence, at the constant applied load, this effect translates to increased film thickness, hence reduced friction as evident from both experimental measurement and numerical predictions (figure 5). This figure provides percentage friction reduction in the textured region with respect to the untreated part of the plate surface. Good qualitative and quantitative comparison is noted between measurements and predictions.

5. ENGINE SIMULATIONS

The numerical model is now used to consider the conditions found in a fired engine. A Honda CRF 450R single cylinder 4-stroke motocross motorbike is modeled. The pertinent data is provided figure 6. Further details about the engine specifications are given in [2].
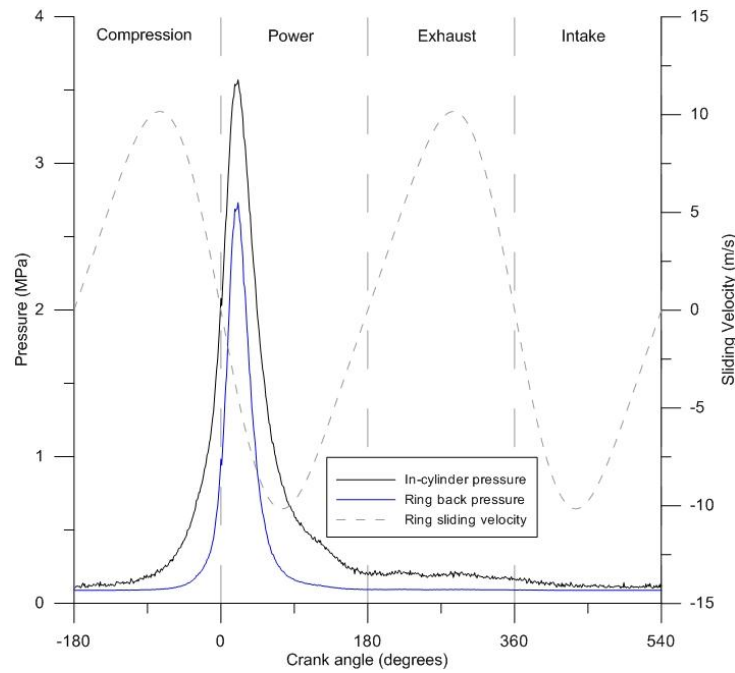
Figure 6: Input data from the Honda CRF 450R engine to the numerical

Similar surface texture designs as those presented in section 2.1 are modelled on the liner 10 degrees crank angle position on the either sides of top dead centre reversal during the transition between the compression to power strokes. During this region, and especially at the beginning of the power stroke when high pressures combine with slow sliding speeds highest frictional losses usually occur.
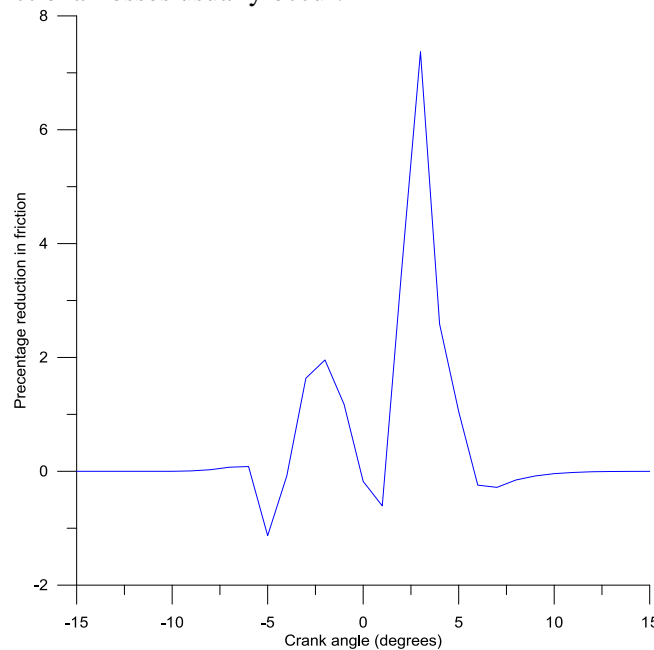

Figure 7: Improvement in friction produced by the surface textures at the end of the compression and beginning of power stroke

The results shown in figure 7 show the reduction in friction with surface texturing included in the analysis relative to untextured surfaces with the same assumed surface topography. The surface textures produce micro-hydrodynamic pressure perturbations as described in the previous section and also reduce the asperity interactions between the contiguous surfaces due to a reduction in contacting area.

6. ACKNOLDGEMENT

REFERENCES

[1]- Etsion I. "Surface texturing for in-cylinder friction reduction" In Tribology and Dynamics of Engine and Powertrain: Fundamentals, Applications and Future Trends. Rahnejat H, Ed. New Delhi (India): Woodhead Publishing Ltd., 2010: 458–469.

[2]- Howell-Smith, S., Rahnejat, H., King, P.D. and Dowson, D., "Reducing in-cylinder parasitic losses through surface modification and coating", Proc. IMechE, Part D: J. Automobile Eng., 228 (4), 2014, pp. 391-402

[3]- Greenwood, J. A., and Tripp, J. H. (1970- 1971) "The Contact of Two Nominally Flat Rough Surfaces,". Proc. IMechE., 185, pp. 625-633.

[4]- Andersson BS. "Company's perspective in vehicle tribology" in Dowson D, Taylor CM, Godet M, editors. Proc. 18th Leeds-Lyon Sympos. Elsevier; 1991, pp. 503-506.

[5]- Gohar, R. and Rahnejat, H., "Fundamentals of Tribology", Imperial College Press, London, 2008

[6]- Mishra, P.C., Rahnejat, H. and King, P.D., "Tribology of the ring—bore conjunction subject to a mixed regime of lubrication", Proc. IMechE, Part C: J. Mech. Eng. Sci., 223(4), 2009, pp. 987-998

[7]- Etsion, I., and E. Sher. "Improving fuel efficiency with laser surface textured piston rings." Tribology International 42(4), 2009, pp. 542-547.

[8]- Ronen, Aviram, Izhak Etsion, and Yuri Kligerman. "Friction-reducing surface-texturing in reciprocating automotive components." *Tribology Transactions* 44.3 (2001): 359-366.

[9]- Rahnejat, H., Balakrishnan, S., King, P.D. and Howell-Smith, S., "In-cylinder friction reduction using a surface finish optimisation technique", Proc. IMechE, Part D: J. Automobile Engineering, 220, 2006, pp. 1309-1318

[10]- De la Cruz, M., Gore, M., Morris, N. and Rahnejat, H. "The role of laser surface textured patterns on friction in reciprocating contacts", Proc. ASME/STLE 2012 International Joint Tribology Conference, IJTC2012:61149, 2012, Denver, Colorado.

[11]- Gore M, Rahnejat H, King P, Theaker M and Howell Smith S "Direct measurement of piston friction of internal-combustion engines using the floating-liner principle" Proc. IMechE, Part D: J. Automobile Engineering, 2013, doi: 10.1177/0954407013511795

[12] Costa, H. L., and I. M. Hutchings. "Hydrodynamic lubrication of textured steel surfaces under reciprocating sliding conditions." *Tribology International* 40.8 (2007): 1227-1238.

[13]- Balakrishnan, S., Howell-Smith, S. and Rahnejat, H., "Investigation of reciprocating conformal contact of piston skirt-to-surface modified cylinder liner in high performance engines", Proc. IMechE, Part C: J. Mech. Engineering Science, 219, 2005, pp. 1235-1247

[14]- Dwyer-Joyce, R.S., Green, D.A., Balakrishnan, S., et al., "The measurement of liner-piston skirt oil film thickness by an ultrasonic means", SAE Int., Technical Pap.: 2006-01-0648, 2006

[15]- Teodorescu M, Kushwaha M, Rahnejat H. and Rothberg, S.J., "Multi-physics analysis of valve train systems: from system level to micro-scale interactions", Proc. IMechE, Part K: J Multi-body Dynamics, 221, 2007, pp. 349–360.

Nomenclature

A	Apparent Contact Area	q,r,f,g,s	Ring profile co-efficients
A_a	Asperity Contact Area	t	Time
B	Ring Face Width	U_1, U_2	Ring, liner speed of entraining motion
E'	Effective Elastic modulus of the contacting pair	V_1, V_2	Ring, liner speed in the axial direction
f_b	Boundary Friction	W_a	Load share of asperities
f_t	Total Friction	W_h	Hydrodynamic Load share
f_v	Viscous Friction	W_T	Total load carried
H	Film Thickness	x	Direction along the ring face(in the direction of entraining motion)
h_0	Minimum Film thickness		
h_s	Profile of the ring face width	x_c	Film rupture boundary
h_t	Surface Feature film thickness	x_m	Centre or the chevron at each cross section
h_d	Chevron Height	y	Direction axially along the ring
l	Ring Length		
l_c	Chevron thickness		Greek Symbols
p	Pressure	η	Lubricant dynamic viscosity
p_c	Cavitation Pressure	κ	Average Asperity tip
p_{in}	Inlet Pressure	λ	Stribeck oil film parameter
		ρ	Lubricant Density